JOURNAL OF GEOPHYSICAL RESEARCH, VOL. 104, NO. C11, PAGES 25,707–25,719, NOVEMBER 15, 1999

Numerical study on signatures of atmospheric convective cells in radar images of the ocean

Susanne Ufermann[1] and Roland Romeiser
Institute of Oceanography, University of Hamburg, Hamburg, Germany

Abstract. Current and wind variations at the ocean surface can give rise to a modulation of the sea surface roughness and thus become visible in radar images. The discrimination between radar signatures of oceanic and atmospheric phenomena can be quite difficult, since signatures of different origin can have very similar shapes and magnitudes and are often superimposed upon each other. In this work we employ a numerical radar imaging model for an investigation of typical properties of radar signatures of atmospheric convective cells and of theoretical differences between such atmospherically induced radar signatures and those of oceanic phenomena. We show that main characteristics of observed multifrequency/multipolarization radar signatures of atmospheric convective cells over the Gulf Stream are reproduced quite well by the proposed model. This encourages us to vary wind and radar parameters systematically in order to get a general overview of the dependency of atmospherically induced radar signatures on these parameters. Finally, we compare typical characteristics of radar signatures of atmospheric and oceanic phenomena, and we present simulated radar images of a scenario of superimposed atmospheric convective cells and oceanic internal waves. We show that the proposed model supports the experimental finding that radar signatures of oceanic phenomena are stronger at horizontal (HH) than at vertical (VV) polarization, while atmospherically induced radar signatures are better visible at VV polarization.

1. Introduction

It is well known that mesoscale atmospheric phenomena over the ocean can modulate the sea surface roughness and thus become visible on radar images, as discussed, for example, for atmospheric convection rolls by *Fu and Holt* [1982], *Thompson et al.* [1983], and *Alpers and Brümmer* [1994], for atmospheric gravity waves by *Thomson et al.* [1992] and *Alpers and Stilke* [1996], and for atmospheric convective cells by *Mitnik* [1992], *Mityagina et al.* [1996], and *Lavrova et al.* [1998]. The theoretical understanding of the radar imaging mechanism of such phenomena can be of vital importance for marine meteorologists and oceanographers who study the phenomena themselves or would like to separate atmospherically induced radar signatures from those resulting from oceanic phenomena. Until now, most of the above mentioned papers have concentrated on analyses of a few particular radar images on the basis of empirical models that relate backscattered radar intensities to wind vectors. Although their results show that the radar imaging mechanism of mesoscale atmospheric phenomena over the ocean is basically understood, general conclusions regarding the dependency of the radar signatures on characteristic parameters of the atmospheric phenomena as well as on radar parameters like the frequency, polarization, or incidence angle could not be drawn.

The main purpose of this work is a more comprehensive investigation of the theoretical radar signatures of mesoscale atmospheric phenomena on the basis of a composite surface radar backscattering model in combination with a model that describes the modulation of the ocean surface wave spectrum by spatially varying wind and current fields at the sea surface. The study concentrates on radar signatures of atmospheric convective cells, which are well visible in multifrequency/multipolarization radar images of the Gulf Stream from the Spaceborne Imaging Radar-C/X-Band Synthetic Aperture Radar (SIR-C/X-SAR) mission. As an example, a synthetic aperture radar (SAR) image that was acquired at L band (1.25 GHz), cross polarization, is shown in Figure 1. The mottled, cloud-like patterns

[1]Now at Southampton Oceanography Centre, Southampton, United Kingdom.

Paper number 1999JC900224.
0148-0227/99/1999JC900224$09.00

Figure 1. SIR-C/X-SAR synthetic aperture radar image of the Gulf Stream edge (L band, HV polarization) off the U.S. east coast, acquired on April 17, 1994, at 1622 UTC, showing signatures of sea surface manifestations of atmospheric convective cells. Size of the imaged area is 20 km × 100 km; incidence angle at image center is 31°.

toward the center of the image indicate our study area, whereas the bright line north of them marks the position of the Gulf Stream front whose radar signature is discussed by *Ufermann and Romeiser* [this issue].

In section 2 we present the parameterization of the wind field of atmospheric convective cells used in this investigation as well as the basic elements of the proposed radar imaging model. In section 3 we show that basic characteristics of the observed radar signatures of atmospheric convective cells in the SIR-C/X-SAR data set, including their dependence on radar frequency and polarization, are reproduced by the proposed model suite. This encourages us to discuss the dependence of simulated radar signatures on parameters of the wind field and on the frequency, polarization, and incidence angle of the radar in a more general way in section 4. Finally, in section 5 we focus on differences between the variations of radar signatures of atmospheric and oceanic origin with polarization. We show that the experimental finding that radar signatures of oceanic phenomena are stronger at horizontal (HH) than at vertical (VV) polarization, while atmospherically induced radar signatures appear to be better visible at VV polarization, is basically consistent with predictions of the proposed model. A summary of our results and conclusions are presented in section 6.

2. Theory

2.1. Wind Field

Atmospheric convective cells over the ocean can be formed where a negative air-sea temperature difference gives rise to unstable stratification of the marine atmospheric boundary layer (MABL) and thus to a pronounced energy exchange in vertical direction. As discussed by *Mitnik* [1992], typical convective cells are characterized by a cylindrical flow pattern which is superimposed upon the ambient wind field. The direction of the cellular air flow directly above the sea surface is either radially outward from the center of the cells ("open cells") or from the rim toward the center ("closed cells"). Adopting an expression from *Mitnik* [1992], we parameterize the surface wind field associated with an open cell by

$$W_c^{\text{open}}(r) = \begin{cases} \frac{r}{r_0} W_c^{\max} & 0 \le r < r_0 \\ \frac{R-r}{R-r_0} W_c^{\max} & r_0 \le r \le R \end{cases} \quad (1)$$

where W_c^{open} represents the local radial wind speed as function of the distance from the cell center r, R is the radius of the cell, r_0 is $5/6R$, and $W_c^{\max}$ denotes the maximum value of cellular wind speed. For the surface wind field of a closed cell we use the functional dependence on r used by *Trump et al.* [1982]:

$$W_c^{\text{closed}}(r) = -W_c^{\max} \sin \frac{\pi r}{R} \quad 0 \le r \le R \quad (2)$$

Examples of surface wind fields of open and closed convective cells produced this way are shown in Figure 2, where Figures 2a and 2c show the wind fields above the sea surface (at the bottom of the cells) as seen from above. Wind vectors are plotted at every fifth

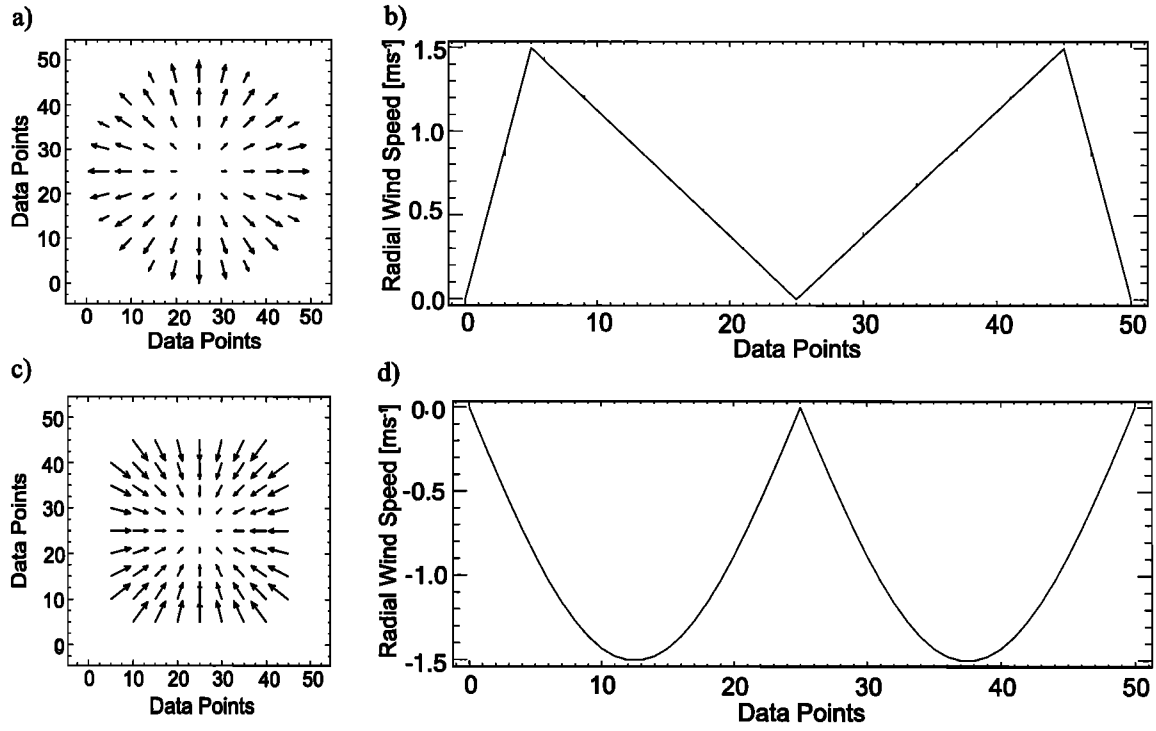

Figure 2. Simulated wind fields of open (Figures 2a and 2b) and closed (Figures 2c and 2d) atmospheric convective cells for a 51×51 data points grid. (a) and (c) Wind fields at the bottom of a convective cell, directly above the sea surface as seen from above; (b) and (d) Magnitude of the wind speed along cuts through the centers of Figures 2a and 2c, respectively.

line/column of a grid of 51×51 points which is the standard model grid for the investigations in sections 3 and 4. Furthermore, Figures 2b and 2d show the magnitude of the wind speed along cuts through the centers of both cells.

2.2. Spatially Varying Surface Wave Spectrum

In contrast to previous studies on this subject which were based on empirical models for the relationship between wind speed and normalized radar backscattering cross section (NRCS), a more "physical" radar imaging model will be employed in this investigation, which accounts explicitly for the spatial variations of the ocean wave spectrum in the presence of wind variations associated with atmospheric convective cells and for the corresponding variations of the backscattered radar signal. This approach allows a physically consistent prediction of radar signatures at various radar frequencies, polarizations, and incidence angles, while investigations on the basis of empirical relations between wind vector and NRCS are normally limited to small parameter ranges for which these relations are valid. Possible failure of the model to reproduce characteristic properties of observed radar signatures will reveal shortcomings in its physical formulation.

The part of the imaging model which is used for the computation of modulated surface wave spectra has been described in detail by *Romeiser and Alpers* [1997]. The model is based on weak hydrodynamic interaction theory in the relaxation time approximation. That is, ray paths of wave components in a five-dimensional wavenumber-space-time domain are traced back in time, and then an action balance equation is integrated in the forward direction to obtain modulated action spectral densities. This is done for typically 100 wavenumbers and 24 wave directions, yielding a full two-dimensional modulated wave spectrum at each grid point for the radar calculations. Our numerical model was originally implemented for applications involving spatially varying current fields, but it also can be applied to spatially varying winds. In this case the equilibrium spectrum and the relaxation rate that determine the source function of the action balance equation vary along the integration path because they are functions of wind speed and direction. This is a simplification compared to dedicated wave prediction models, which treat the physics of the generation and decay of (long) ocean waves more explicitly, but it appears reasonable as long as we are mainly interested in intensity variations of relatively short waves on scales that are much longer than their wavelengths. Advantages of the proposed numerical model are that it is efficient in terms of computation time, that it allows a consistent simulation of individual effects of wind and current variations,

and that it can be applied to scenarios of combined spatially varying wind and current fields, like the scenario discussed in section 5.

Parameterizations of the two-dimensional equilibrium wave spectrum and relaxation rate used in the proposed model are given by *Romeiser et al.* [1997] and by *Romeiser and Alpers* [1997], respectively.

2.3. Radar Backscatter

The radar backscattering model used for this study is a composite surface model based on a Taylor expansion of the NRCS as given by Bragg scattering theory [*Wright,* 1968; *Valenzuela,* 1978]. Contributions of the whole two-dimensional ocean wave spectrum to the radar backscatter are taken into account. A detailed description of the model was given by *Romeiser et al.* [1997], who showed that it reproduced basic dependencies of mean measured NRCS values for wide ranges of radar parameters (frequency, polarization, incidence angle) and wind speeds and directions quite well. Assuming that realistic intensity variations of short- and intermediate-scale ocean waves are obtained from the wave model described above, one can expect that the scattering model will convert these intensity variations into realistic NRCS variations.

3. Model Validation

3.1. Reference Data Set

Within the framework of the first SIR-C/X-SAR mission a set of radar images of the northwestern edge of the Gulf Stream off the U.S. east coast was acquired on April 17, 1994, 1622 UTC. Two SAR sensors (SIR-C, operating at L and C band, and X-SAR, operating at X band) were mounted aboard the U.S. space shuttle Endeavour during this 10-day campaign to acquire two-dimensional high-resolution multifrequency/multipolarization radar images of the Earth's surface under various incidence angles. The radar images of the Gulf Stream edge which are used for our study were acquired at the frequencies 1.25 GHz (L band) and 5.30 GHz (C band) in VV, HH, and HV ("cross") polarization and at 9.60 GHz (X band) in VV polarization. Thus a set of seven individual images of the same scene is available for analysis, which is shown in Figure 3.

On the day of the shuttle overflight, in situ measurements in the region of the Gulf Stream edge were performed by the Naval Research Laboratory (NRL) from a research vessel equipped with a serial ASCII instrumentation loop (SAIL) data acquisition system. Using this instrumentation, sea surface salinity and temperature, wind speed and direction, and air pressure and temperature were sampled at a rate of one data record per minute. The data used in the following were acquired ~2 hours before the shuttle overflight as a scan perpendicular to the Gulf Stream front, crossing the front from northwest to southeast.

As shown in Table 1, the same mean wind vector was encountered both inside and outside the Gulf Stream region, whereas the difference between measured air and sea surface temperatures changes significantly across the front. The data indicate a stable thermal stratification of the MABL outside the Gulf Stream, whereas the warm waters of the Gulf Stream cause an unstable thermal stratification in the MABL. This is consistent with Figure 4, which depicts that the measured wind speed over the Gulf Stream exhibits strong fluctuations, indicating turbulence and, very likely, the existence of atmospheric convective cells.

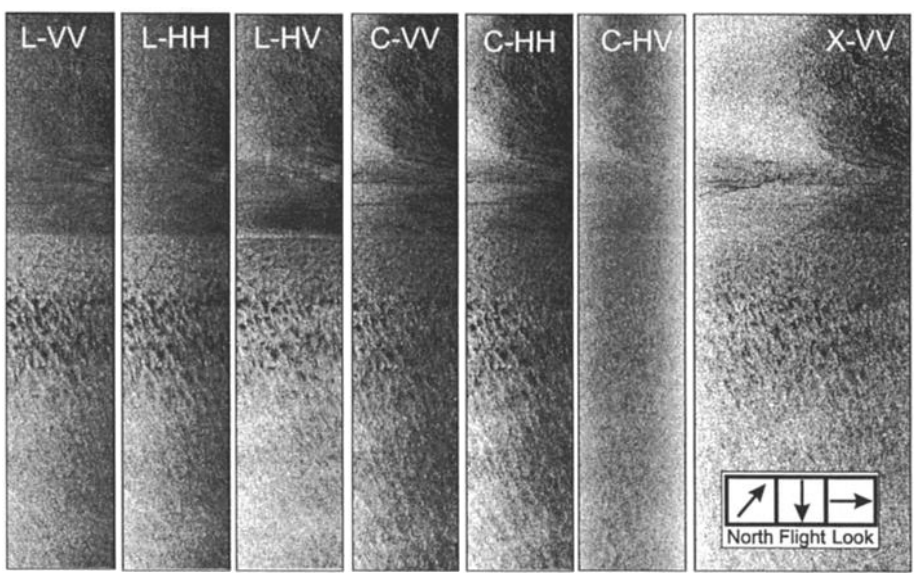

Figure 3. Full set of SIR-C/X-SAR images of the same scene at the Gulf Stream edge acquired on April 17, 1994, at 1622 UTC (see Figure 1). Size of imaged area is 20 km × 100 km for L and C band and 40 km × 100 km for X band.

Table 1. Temperature and Wind Data Inside and Outside of the Gulf Stream From In Situ Measurements

	Inside Gulf Stream	Outside Gulf Stream
SST	23°C	10°C
Air temperature	16°C	15°C
Mean wind speed	3.5 $m s^{-1}$	3.5 $m s^{-1}$
Wind direction	130° (SE)	130° (SE)

The region of pronounced wind speed fluctuations corresponds to the region in the radar image of Figure 1, which is characterized by a mottled pattern of high and low NRCS values. This test area for our investigations is shown in detail in Figure 5. The radar signatures exhibit a regular pattern of roughly circular-shaped features. Alternating regions of high and low backscatter indicate corresponding variations of the surface roughness and thus the wind speed, which is consistent with the in situ data as well as with the theory of atmospheric convective cells. This justifies the assumption that the mottled radar signatures result from sea surface manifestations of atmospheric convective cells. In addition, we conclude from the facts that the measured ambient wind is directed approximately from the lower right of Figure 5 toward the upper left and that bright lower right and dark upper left corners of the cellular radar signatures indicate maximum and minimum total wind speeds at these locations, that the circulation pattern of the atmospheric convective cells must be of "closed" type.

3.2. Model Results for the Test Scenario

For direct comparison between SIR-C/X-SAR data and model results, one of the pronounced cell features in the upper part of Figure 5 was selected. Figure 6 (left) shows measured radar signatures of this feature at all available frequencies and polarizations. For best visualization of their characteristics and differences the signatures are represented by NRCS isolines in steps of −1 dB, starting from the maximum NRCS value of each individual image.

Figure 6 (right) shows the model results for parameter settings with an ambient wind speed of 3.5 $m s^{-1}$, a maximum cellular wind speed W_c^{max} of 1.5 $m s^{-1}$, a cell radius R of 1000 m, and an incidence angle of 31°. The ambient wind direction is set to come from 110° with respect to north (110°N), which is slightly off the reported in situ measured mean value of 130°N but leads to best agreement between simulated and observed signatures. In Figure 6 the wind direction of 110°N corresponds to an angle of 150° clockwise from the top of the images, since all images are aligned with the flight direction toward 140°N.

Although the simulated radar signatures look, as one might expect, somewhat idealized compared to the more irregularly shaped measured ones, the observed and simulated radar signatures show clear qualitative similarities. This is not true for C band, HV polarization, but the C-HV image looks generally blurred

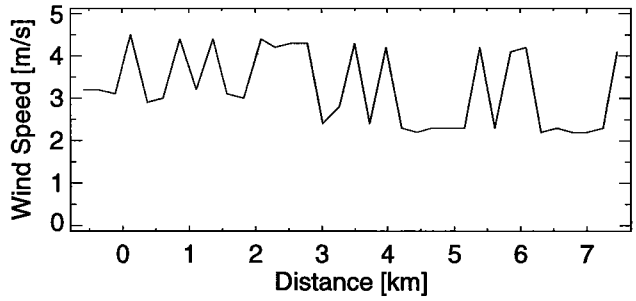

Figure 4. Wind speed according to in situ measurements over the Gulf Stream, showing fluctuations caused by atmospheric convective cells (Gulf Stream front approximately at 0 km).

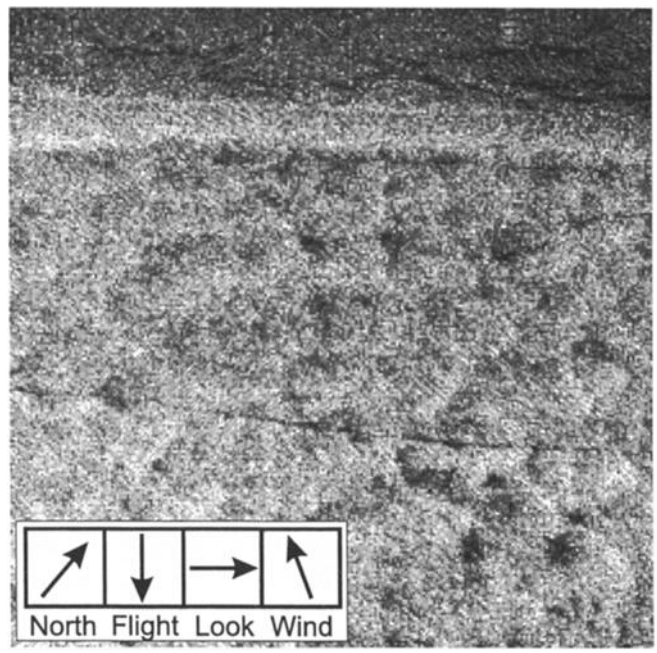

Figure 5. Detail of the SIR-C/X-SAR image (L-HV) shown in Figure 3. Size of the imaged area is 12.5 km × 12.5 km.

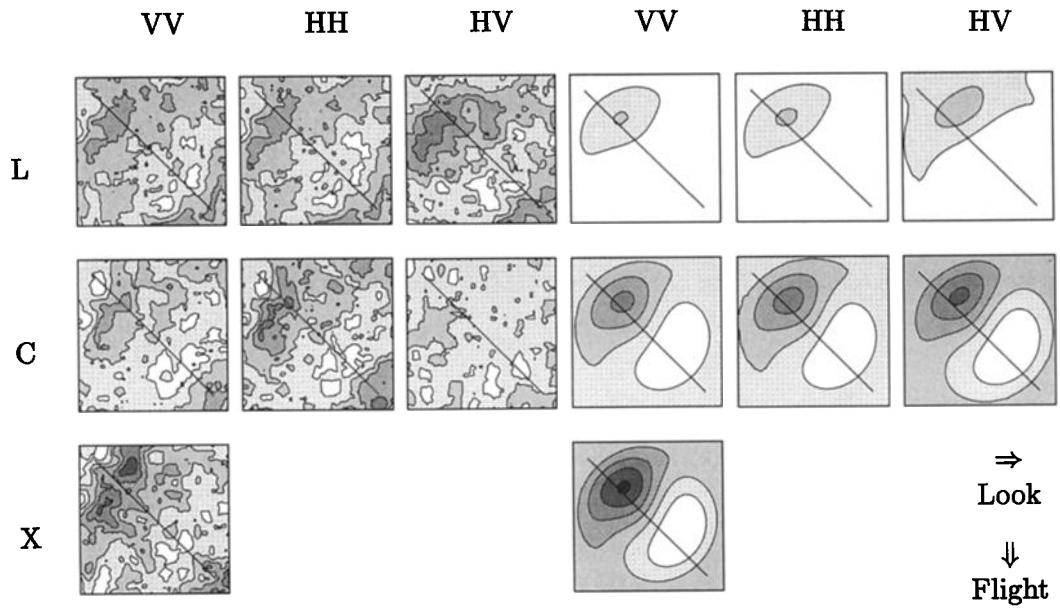

Figure 6. (left) Observed and (right) simulated radar signatures of one of the convective cells of Figure 5. NRCS isolines are plotted in steps of −1 dB starting from the maximum value of each individual image. Diagonal lines mark the position of an intensity scan (see Figure 7).

and has clearly less contrast than the images from all other channels (see Figure 3). We believe that this results from a technical problem rather than from an actual effect in the radar imaging mechanism. At the other six channels a diagonal orientation of the convective cell signatures, an increase of the modulation depth with radar frequency, very similar signatures at VV and HH polarization, and a larger modulation at L band HV, compared to VV and HH, are consistently found in data and model results.

For an analysis from another perspective, plots of image intensity scans along the diagonal line through each radar signature of Figure 6 were produced. These plots, examples of which are shown in Figure 7, show that the shapes of observed NRCS variations in radial direction as well as absolute modulation depths are reproduced quite well by the model at the two higher radar frequencies (C and X band). Also a trend of the measured radar signatures to become stronger with increasing radar frequency and a tendency of their dark regions to become wider at the same time are basically consistent with model predictions.

Only the frequency dependence of the modulation depth is found to be overestimated by the model, which results in an underestimation of the measured L band signatures. Predicted and measured modulation depths at L band VV are ~2 dB and ~3 dB, respectively; that is, the model predicts a ratio of ~1.6 between the brightest and the darkest area, while the data suggest a ratio of ~2.0. There are several possibilities to correct a discrepancy like this by tuning the wind field, the wind dependence of the wave spectrum, the relaxation rate, or the form of the source function of the action balance equation in our wave model. However, in view of the facts that the model results are not too bad without tuning and that reference wave data from the test site are not available, we refrain from a dedicated tuning procedure in the context of this work. In addition, some discrepancy between observed and simulated L band signatures may result from the effect of wind-induced surface current variations underneath the atmospheric convective cells, which is completely omitted in our present model: Surface current gradients can give rise to a hydrodynamic modulation of surface waves in addition to the aerodynamic modulation by the wind field itself. As shown by *Romeiser and Alpers* [1997] and by *Ufermann and Romeiser* [this issue], the hydrodynamic modulation of Bragg waves is usually more pronounced at L band than at C and X band.

Another discrepancy between measurements and model results that may require a brief discussion is a general overestimation of absolute NRCS values in all bands and polarizations by our model. This is an instrument-specific phenomenon, which is already known from other studies. It can be explained by differences in the calibration of radar data from different sources and comparable uncertainties in the parameterization of the ocean wave spectrum. As shown by *Romeiser et al.* [1997], measured absolute NRCS values can, in principle, be reproduced by the proposed model after some optimization of the wave spectrum within limits determined by existing parameterizations from the literature. The model results presented in this work have been obtained with a "default" wave spectrum obtained in the above mentioned study on the basis of airborne scatterometer data. Using this wave spectrum, NRCS values from

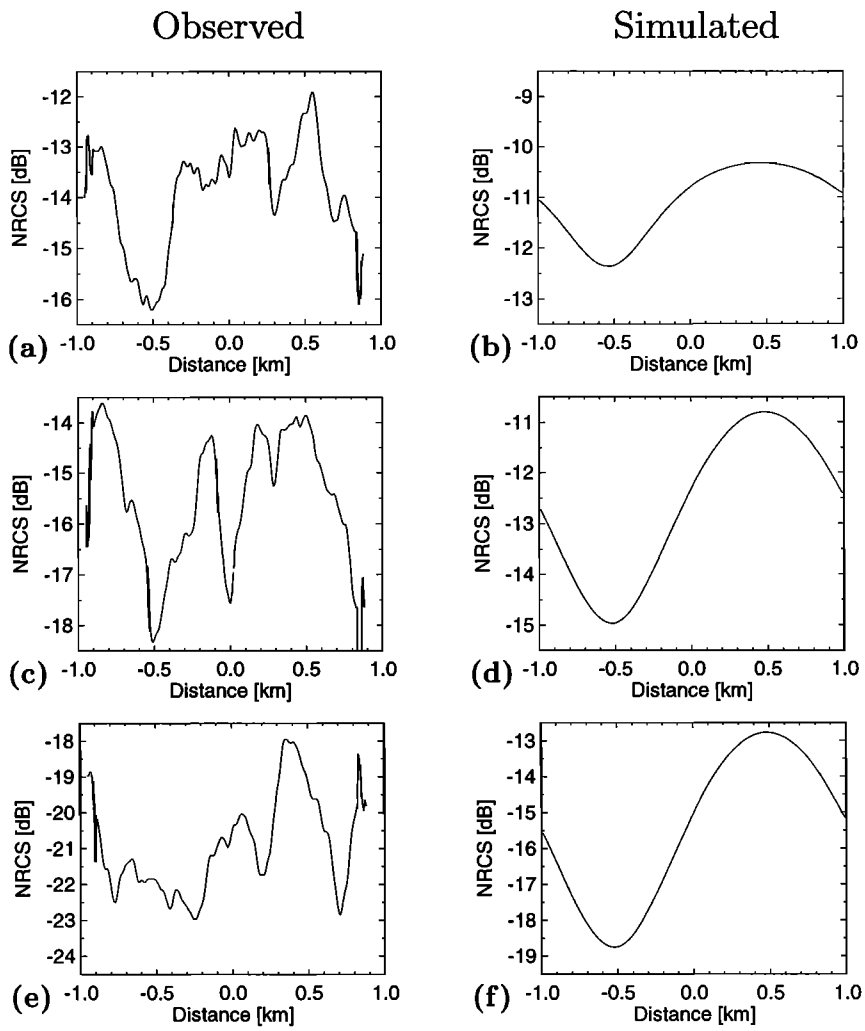

Figure 7. Intensity scans through the observed (Figures 7a, 7c, and 7e) and simulated (Figures 7b, 7d, and 7f) radar signatures of atmospheric convective cells along the diagonal lines shown in Figure 6; (a) and (b) L-VV; (c) and (d) C-VV; and (e) and (f) X-VV.

spaceborne systems like ERS 1, ERS 2, and SIR-C/X-SAR are consistently found to be overestimated, which suggests that the wave spectrum should be recalibrated. However, absolute NRCS values are only a side issue of the discussion in this work, and small modifications of the wave spectrum would have only minor effects on relative NRCS variations. Our findings regarding shapes and modulation depths of simulated radar signatures and their general dependencies on several parameters are thus quite robust, and the encountered differences of the order of 3 dB between measured and simulated absolute NRCS values do not indicate a fundamental problem of our theory.

4. Sensitivity Analysis

4.1. Motivation

Having demonstrated that the proposed radar imaging model is capable of explaining main characteristics of some particular observed radar signatures of atmospheric convective cells, we can employ the model for a systematic study on the variations of such radar signatures with the involved key parameters. Main goals of this study are to identify parameter combinations for which particularly strong or weak radar signatures of wind variations over the ocean can be expected, to get an impression of the variability of such signatures with various parameters, and to determine what conclusion regarding the physical properties of a given wind feature can be drawn from its radar signatures.

We have simulated radar signatures of open and closed atmospheric convective cells for several ambient wind speeds (0.0, 1.5, 3.5, 10.0 $\mathrm{m\,s^{-1}}$), wind directions (0°–360° in steps of 45°), radar frequencies (1.25, 5.30, 9.60 GHz), polarizations (VV, HH, HV), and incidence angles (30° and 40°). In total, 720 different radar signatures were simulated, which are shown completely by *Ufermann* [1998]. Results of the analysis of those signatures are summarized in section 4.2.

4.2. Results

The model results reveal that the interpretation of radar signatures of atmospheric convective cells can be quite difficult due to a number of ambiguities. For example, an increase of the NRCS can be caused by an increase in wind speed, by a variation of the angle between ambient wind and radar look direction, or by a decrease of the radar incidence angle. Fortunately, radar properties such as the incidence angle are usually well defined, which reduces the possible ambiguities in practical applications.

The main characteristics of the simulated radar signatures can be summarized as follows:

1. NRCS isolines of open cells are crescent-shaped with their maximum values at a distance of $\sim 5/6R$ from the cell center (see Figure 8a), whereas those of closed cells are kidney-shaped with their maximum values at a distance of $\sim 1/2R$ from the cell center (see Figure 8b).

2. The modulation depth decreases with increasing ambient wind speed (e.g., for L band VV polarization, at an incidence angle of 30° and an angle of 135° between wind and look direction: 8.5 dB modulation depth at an ambient wind speed W_a =1.5 ms^{-1} to 2.1 dB at W_a =3.5 ms^{-1} to 0.4 dB at W_a =10.0 ms^{-1}), while the NRCS isolines change their shape from "circular" via "crescent" to "semicircular/ oval".

3. The angle between ambient wind and radar look direction strongly influences the shape of the NRCS isolines; particularly at high wind speeds and radar frequencies it influences the absolute NRCS values (up to 5 dB difference), and (particularly at low wind speeds) it influences the orientation of the radar signatures.

4. Modulation depth increases with radar frequency (see Figure 9).

5. There are hardly any differences between signatures at VV and HH polarization (see Figures 10a and 10b); HV polarization signatures show a larger modulation depth and differently shaped NRCS isolines, but they are associated with very low absolute NRCS values (see Figure 10c).

6. The incidence angle determines most strongly the mean absolute NRCS values at HH polarization (up to 8 dB difference between maximum and minimum NRCS obtained in our calculations); absolute NRCS values are larger at smaller incidence angles. A strong variation of the modulation depth with varying incidence angles is not found.

We conclude from these findings that a radar operating at a high frequency should be best suited for the detection of atmospheric convective cells. A moderate incidence angle as well as vertical (VV) or horizontal (HH) polarization should be used in order to avoid problems arising from low backscattered power at large incidence angles or at cross polarization. Owing to reasons explained in section 5, VV polarization appears to be actually most favorable for meteorological investigations. We would like to point out in this context that our results are basically consistent with findings of *Mitnik* [1992], but our employment of a "physical" radar imaging model allows us to consider extended parameter ranges (e.g., three radar frequencies instead of one) and the derivation of more general conclusions.

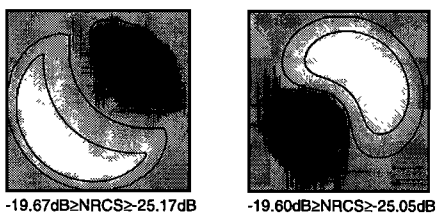

Figure 8. Simulated radar signatures at L band VV polarization of (a) an open atmospheric convective cell and (b) a closed atmospheric convective cell. Look direction is from the bottom/right; incidence angle is 40°; ambient wind speed $W_a = 3.5\ \mathrm{m\,s^{-1}}$ from the top/right; maximum cellular wind speed $W_c^{\max} = 1.5\ \mathrm{m\,s^{-1}}$; size of each simulated area is 2 km × 2 km. Numbers at bottom indicate maximum and minimum absolute NRCS.

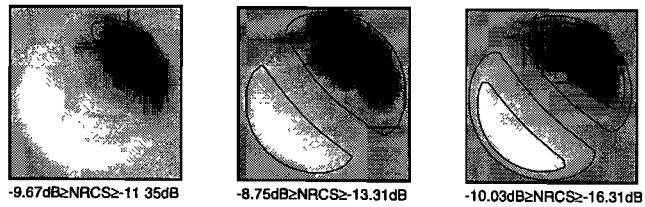

Figure 9. Simulated radar signatures of open atmospheric convective cells for different radar frequencies ((a) L band, (b) C band, and (c) X band) at vertical polarization. Look direction is from the bottom/left; incidence angle is 30°; other parameters are as in Figure 8.

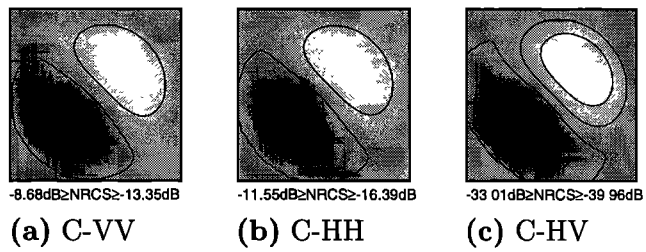

Figure 10. Simulated radar signatures of closed atmospheric convective cells for different radar polarizations ((a) VV, (b) HH, and (c) HV) at C band. Other parameters are as in Figure 9.

5. On the Differences Between Radar Signatures of Atmospheric and Oceanic Origin

5.1. Motivation

In the previous sections, we have discussed how radar signatures of atmospheric convective cells over the ocean can be explained by a theoretical model and how such signatures depend on a variety of environmental parameters and radar parameters. We have also discussed what radar parameters should ideally be chosen to detect atmospheric convective cells by radar. However, in typical practical applications, not only radar signatures of atmospheric origin but also signatures resulting from spatial variations in the surface current field may be present in radar imagery. Oceanographers and marine meteorologists who work with such data need to separate signatures of atmospheric and oceanic origin, which can be difficult in some cases. For example, internal waves in the atmosphere can give rise to radar signatures that are very similar to those of internal waves in the ocean [*Alpers*, 1995; *Alpers and Stilke*, 1996]. It would be convenient if multipolarization or multifrequency radar images could be exploited to discriminate between features of different nature whose radar signatures look similar on a single image.

Existing multipolarization radar imagery from several experimental campaigns suggests that the backscattered signal is more sensitive to wind variations at VV than at HH polarization, while oceanic features like internal waves or the bathymetry in coastal waters are often better visible at HH. An impressive example of a pair of images which exhibit such behavior is shown in Figure 11: While strong signatures of oceanic internal waves can be seen in the HH image, the corresponding VV image is clearly dominated by signatures of superimposed atmospheric convective cells. These and similar other images were obtained from a Russian airborne real aperture radar during the Joint U.S./Russia Internal Wave Remote Sensing Experiment (JUSREX-92) in the New York Bight [*Etkin et al.*, 1994; *Gasparovic and Etkin*, 1994; *Mityagina et al.*, 1996; *Lavrova et al.*, 1998]. The radar frequency is 13.3 GHz (K_u band), and the incidence angle is ~80° at the image center.

The observation that radar signatures of atmospheric phenomena are better visible at VV than at HH polarization appears to contradict our findings from section 4. We will show in the following that this is not necessarily true, and we will discuss mechanisms that can cause pronounced differences between radar signatures of oceanic and atmospheric phenomena at different polarizations within the framework of the proposed model. Although these mechanisms may be different from the ones that are actually responsible for the JUSREX-92 observations (and not yet understood), our results support the conclusion that radar signatures of oceanic and of atmospheric phenomena are more pronounced at HH and at VV polarization, respectively.

5.2. Model Predictions

As briefly indicated in section 2, the radar imaging model used in this work is based on an expression for the NRCS of the ocean surface which consists of a zeroth-order term given by resonant Bragg scattering theory [*Wright*, 1968; *Valenzuela*, 1978] and a number of terms of second order in the surface slope. The second-order

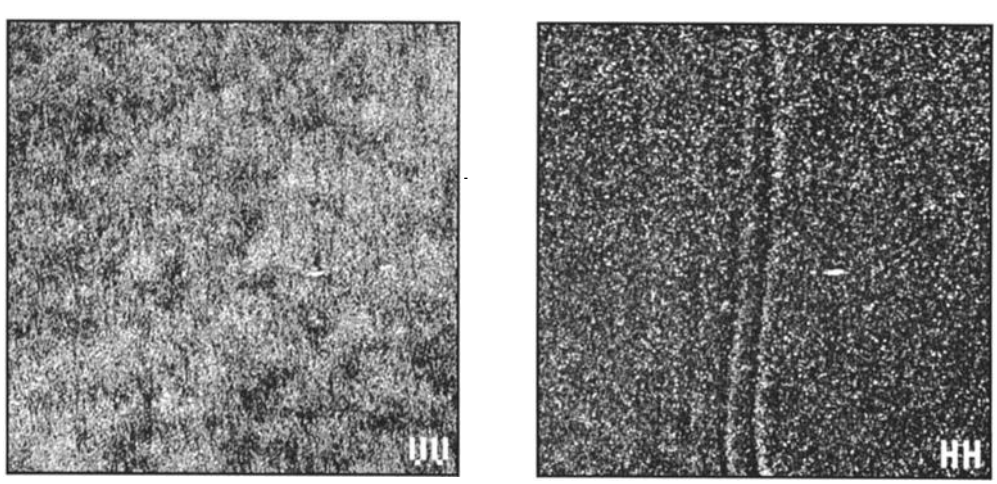

Figure 11. Pair of real aperture radar images obtained simultaneously at VV and HH polarization during JUSREX-92, showing signatures of an internal wave feature and superimposed atmospheric convective cells. Approximate size of imaged areas is 8 km × 8 km; radar frequency is 13.3 GHz; incidence angle at image center is 80°; and look direction is from bottom to top of figure (downwind).

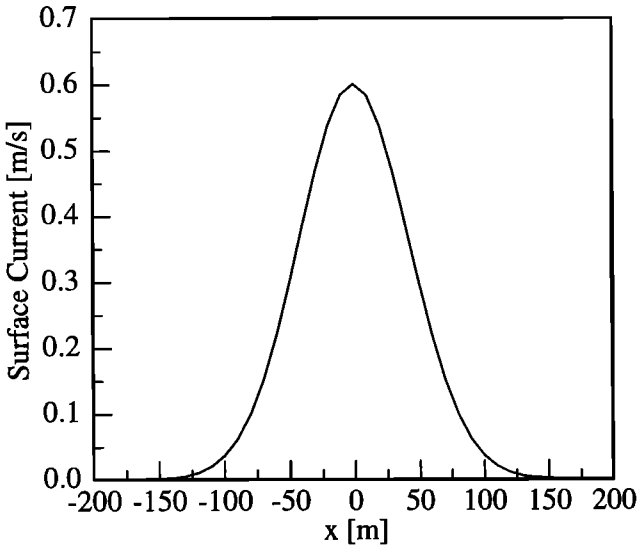

Figure 12. Idealized surface current field over a typical oceanic internal wave encountered during JUSREX-92.

terms account for the impact of waves that are long compared to the short Bragg waves which are in resonance with the radar signal. As shown by *Romeiser and Alpers* [1997], their relative contribution to the NRCS is larger at HH than at VV polarization. The second-order terms are proportional to the mean square surface slope. In addition, second- and zeroth-order terms are proportional to the wave height spectral density of the Bragg waves. The latter explains why wind variations within relatively short spatial scales, which modulate mainly short surface waves, give rise to similar radar signatures at VV and HH polarization, as shown in sections 3 and 4. In contrast, the hydrodynamic modulation associated with oceanic phenomena affects mainly longer waves of wavelengths between decimeters and meters, whose intensity variations affect only the second-order terms of the NRCS, so that polarization-dependent signatures are obtained. Accordingly, our imaging model predicts more pronounced differences between radar signatures of oceanic phenomena at VV and HH polarization than between those of atmospheric phenomena.

According to available data [*Gasparovic and Etkin*, 1994; Y. Trokhimovski, personal communication, 1997], typical surface currents over internal solitons like the ones of Figure 11 can be approximated by a Gaussian function with a peak current of up to 0.6 $\mathrm{m\,s^{-1}}$ and a width of about 200 m, as plotted in Figure 12. The phase speed of the internal wave is $\sim$0.7 $\mathrm{m\,s^{-1}}$ toward positive x direction in this plot. Calculating hydrodynamically modulated surface wave spectra across this current field and the corresponding NRCS as function of x, one obtains radar signatures with a positive modulation at the forward face of the internal wave (positive x values in Figure 12) and a negative modulation behind its crest (negative x values). A modulation depth can be defined which relates the maximum NRCS value of a simulated signature to the minimum value. Figure 13 shows such modulation depths as function of the direction of propagation of the internal wave with respect to the radar look direction and for VV and HH polarization. In order to resemble the JUSREX-92 scenario of Figure 11 as closely as possible, the model runs were performed for a radar frequency of 15.0 GHz and an incidence angle of 65° , where the latter value was chosen significantly smaller than the nominal 80° in order to avoid validity problems with the composite surface model. That is, the proposed model in its present form is not applicable to the actual scenario of Figure 11 and thus not expected to reproduce the observations perfectly, but we can apply the model to a similar scenario for which it should be valid and see if similarities between measured and obtained polarization dependence are obtained. In all model runs for the generation of Figure 13, the wind speed was assumed to be 5 $\mathrm{m\,s^{-1}}$, blowing down the radar look direction.

The model results indicate that the JUSREX-92 internal wave features should be clearly better visible at HH than at VV polarization. The difference between modulation depths at HH and VV is >2 dB for an internal wave propagating toward the radar (180° in Figure 13). At directions of 90° and 270°, corresponding to the actual geometry of Figure 11, the modulation depths at both polarizations have a minimum. However, while the minimum modulation depth at HH polarization is still of the order of 1.5 dB, the signature at VV vanishes almost completely under the same conditions. This behavior results from the fact that the Bragg waves themselves are not modulated at all when

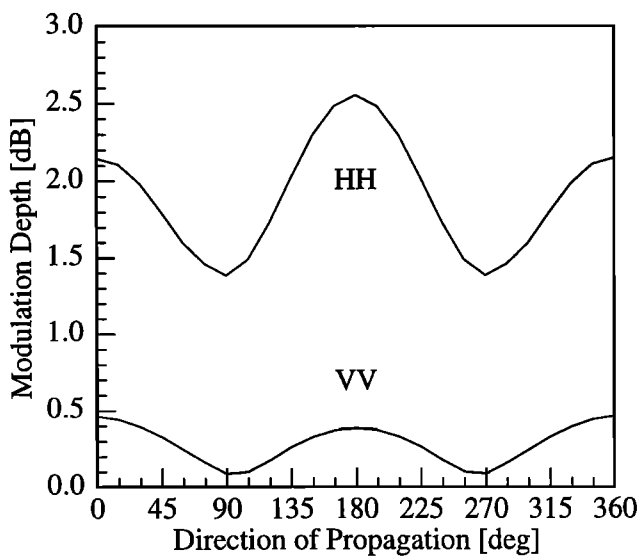

Figure 13. Theoretical modulation depth of a JUSREX-92 internal wave feature as function of the direction of propagation of the internal wave with respect to the radar look direction. Radar frequency is 13.3 GHz; incidence angle at image center is 65°; and wind speed is 5 $\mathrm{m\,s^{-1}}$, blowing down the radar look direction.

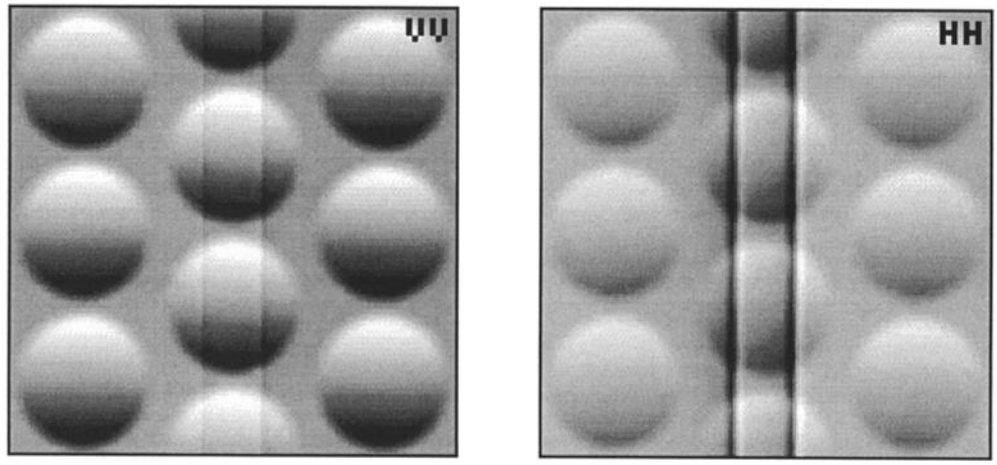

Figure 14. Simulated radar signatures of superimposed oceanic internal waves and atmospheric convective cells at VV and HH polarization for a scenario resembling the scenario of Figure 11. Gray scales have been adjusted individually for each image.

the radar look direction is aligned with the internal wave crest, while the perpendicular longer waves which do experience strong modulation cause a considerable contribution to the NRCS at HH but not at VV polarization.

5.3. Discussion

A preliminary conclusion from these results is that our model can explain the fact that the internal wave features of Figure 11 are better visible at HH than at VV polarization, while it does not appear to be capable of explaining observed stronger signatures of atmospheric features at VV than at HH. However, although quantitative evidence of stronger atmospherically induced radar signatures at VV than at HH, thus evidence of shortcomings of our imaging model, may exist, one should be aware of the fact that printed radar images which appear to exhibit such behavior can be misleading. It is common practice to optimize the gray scales of printed radar images individually in such a way that the darkest and the brightest areas of interest are mapped to gray levels close to black and to white, respectively (in order to account for variations due to speckle noise, one would do this on the basis of intensity histograms). If, by chance, the atmospherically induced signatures in the VV and HH channels of Figure 11 were stronger than the internal wave signatures at VV but weaker than those at VV polarization, gray scale optimization could well have resulted in dynamical ranges which emphasize the internal waves at HH and the atmospheric features at VV. In order to demonstrate this effect, we have produced Figure 14 which shows gray scale-optimized results of a model run based on the aerodynamic and hydrodynamic scenario of Figure 11: The observed internal wave feature has been modeled by a combination of two features according to Figure 12 with a distance of 800 m; the effect of the superimposed wind fluctuations is represented by a couple of open convective cells with a diameter of 2000 m and a wind amplitude of 0.5 $\mathrm{m\,s^{-1}}$ at a mean ambient wind speed of 5 $\mathrm{m\,s^{-1}}$. The simulated images were produced by calculating spatially varying ocean wave spectra in the presence of the combined current and wind variations and feeding them into the composite surface scattering model, assuming again a radar frequency of 15 GHz and an incidence angle of 65°.

Given the facts that our model is not supposed to be valid at an incidence angle of 80° and that absolute NRCS variations of the JUSREX-92 images of Figure 11 have not been available to us, it is difficult to rate the significance of our model results, and we do not intend to say that we can explain the JUSREX-92 findings. However, a qualitative agreement of the differences between the simulated radar images for VV and HH and the differences between the measured ones of Figure 11 is obvious, and to our knowledge, no other theoretical explanation for the polarization effects in the JUSREX-92 data has been given so far in the literature. This encourages us to conclude that (1) the experimental finding that radar signatures of oceanic features are better visible at HH than at VV polarization is in good agreement with predictions of our imaging model; while (2) the impression that radar signatures of spatial wind variations are better visible at VV than at HH polarization is not confirmed by model results, but it may partly result from gray scale optimization of printed radar images in combination with the dominance of superimposed signatures of hydrodynamic features at HH polarization.

On the basis of our model results and the JUSREX-92 observations, we come to the conclusion that radar signatures of oceanic and atmospheric phenomena can, to some extent, be discriminated on the basis of their different variations with the polarization of the radar. In particular, radar signatures of oceanic phenomena

should usually be stronger at HH than at VV polarization. Where only one polarization is available, VV appears to be favorable for studies of wind-induced radar signatures, while HH should be selected for studies focusing on hydrodynamic features. Although the complete explanation for the polarization effects observed during JUSREX-92 may be more complex than the one suggested above, these recommendations appear to be robust, since there is at least qualitative consistency between JUSREX-92 findings and our model results.

6. Summary and Conclusions

In this work we have presented a theoretical model that can be used for the simulation of multifrequency/multipolarization radar signatures of the ocean surface in the presence of features like atmospheric convective cells above the sea surface and superimposed spatially varying current fields. The model consists of a parameterization of the wind field that originates from the convective cells and the ambient wind field, a module for the computation of spatially varying wave spectra for each grid point, and a composite surface model for the computation of radar images. The model has been shown to reproduce main characteristics of existing multifrequency/multipolarization radar signatures of atmospheric convective cells over the Gulf Stream encouragingly well.

In contrast to former approaches based on empirical wind scatterometer models, the "physical" nature of the proposed model has enabled us to investigate the theoretical dependence of radar signatures of atmospheric convective cells on a variety of environmental and radar parameters and to make predictions for parameter combinations for which no experimental findings exist. On the basis of a sensitivity analysis we could show how far parameters of atmospheric convective cells can be determined from radar images and what radar parameters (high frequency, moderate incidence angle, VV or HH polarization) should be chosen for best detection of such features.

Finally, characteristic differences between radar signatures of atmospheric and oceanic phenomena have been discussed. The experimental finding that radar signatures of oceanic features are stronger at HH than at VV polarization, while radar signatures of atmospheric features are better visible at VV than at HH, was shown to be basically consistent with our radar imaging model, although a complete understanding of the JUSREX-92 signatures discussed in section 5 will require further investigations. However, JUSREX-92 data and model results support the conclusion that VV polarization is favorable for the remote sensing of atmospheric phenomena, while HH polarization should be used to observe oceanic phenomena with a minimized impact of superimposed atmospheric phenomena. Furthermore, it seems to be feasible to discriminate signatures of atmospheric and oceanic origin in multipolarization radar images by comparing modulation depths obtained at different polarizations. According to our model, absolute modulation depths associated with atmospheric phenomena should be almost independent of the polarization, while pronounced differences are found in case of oceanic phenomena.

Further work in this field should focus on the development of inverse models, which identify radar signatures of oceanic and atmospheric origin automatically and extract geophysical information from the signatures. In addition, more detailed investigations on the differences between radar signatures at VV and HH polarization should be carried out. We believe that such activities would be quite promising and particularly valuable in view of coming multipolarization spaceborne SAR missions such as Envisat and of a generally growing demand for the operational use of remote sensing techniques.

Acknowledgments. We would like to thank Tim Donato, Scott Chubb, and Farid Askari from NRL (Washington, D.C.) and Yuri Trokhimovski from IKI/RSSI (Moscow, Russia) for providing in situ data, JUSREX-92 imagery, and additional information for this study and our colleagues Martin Gade and Werner Alpers for valuable discussions. This work has been supported by the European Commission, DG XII, as part of the Marine Science and Technology (MAST) program, contract MAS3-CT95-0035 (C-STAR), and by the German Space Agency (DARA) under contract 01QS9016/50QS90165 (X-SAR/SIR-C).

References

Alpers, W., Measurement of mesoscale oceanic and atmospheric phenomena by ERS-1 SAR, *Radio Sci. Bull., 275,* 14-22, 1995.

Alpers, W., and B. Brümmer, Atmospheric boundary layer rolls observed by the synthetic aperture radar aboard the ERS-1 satellite, *J. Geophys. Res., 99,* 12,613-12,621, 1994.

Alpers, W., and G. Stilke, Observation of a nonlinear wave disturbance in the marine atmosphere by the synthetic aperture radar aboard the ERS 1 satellite, *J. Geophys. Res., 101,* 6513-6525, 1996.

Etkin, V. S., Y. Trokhimovski, V. V. Yakovlev, and R. F. Gasparovic, Comparison analysis of Ku-band SLAR sea surface images at VV and HH polarizations obtained during the Joint US/Russia Internal Wave Remote Sensing Experiment, in *Proceedings of the International Geoscience and Remote Sensing Symposium (IGARSS '94),* pp. 744-746, Inst. of Electr. and Electron. Eng., Piscataway, N. J., 1994.

Fu, L. L., and B. Holt, Seasat views oceans and sea ice with synthetic aperture radar, *JPL Publ., 81-120,* 200 pp., 1982.

Gasparovic, R. F., and V. S. Etkin, An overview of the Joint US/Russia Internal Wave Remote Sensing Experiment, in *Proceedings of the International Geoscience and Remote Sensing Symposium (IGARSS '94),* pp. 741-743, Inst. of Electr. and Electron. Eng., Piscataway, N. J., 1994.

Lavrova, O., M. Mityagina, and K. Sabinin, Investigation of perturbing action of atmospheric and internal oceanic processes on the waved sea surface using ocean remote sensing data, in *Proceedings of Oceans '98,* pp. 629-633, Oceanic Eng. Soc., Piscataway, N. J., 1998.

Mitnik, L. M., Mesoscale coherent structures in the surface wind field during cold air outbreaks over the far eastern

seas from the satellite side looking radar, *Mer, 30,* 297-314, 1992.

Mityagina, M. I., Y. A. Kravtsov, V. G. Pungin, K. D. Sabinin, and V. V. Yakovlev, Detection of convective instability in atmospheric boundary layer over the ocean by airborne Ku-band real aperture radar, in *Proceedings of the International Geoscience and Remote Sensing Symposium (IGARSS '96),* pp. 103-105, Inst. of Electr. and Electron. Eng., Piscataway, N. J., 1996.

Romeiser, R., and W. Alpers, An improved composite surface model for the radar backscattering cross section of the ocean surface, 2, Model response to surface roughness variations and the radar imaging of underwater bottom topography, *J. Geophys. Res., 102,* 25,251-25,267, 1997.

Romeiser, R., W. Alpers, and V. Wismann, An improved composite surface model for the radar backscattering cross section of the ocean surface, 1, Theory of the model and optimization/validation by scatterometer data, *J. Geophys. Res., 102,* 25,237-25,250, 1997.

Thompson, T. W., W. T. Liu, and D. E. Weissman, Synthetic aperture radar observation of ocean roughness from rolls in an unstable marine boundary layer, *Geophys. Res. Lett., 10,* 1172-1175, 1983.

Thomson, R. E., P. W. Vachon, and G. A. Borstad, Airborne synthetic aperture radar imagery of atmospheric gravity waves, *J. Geophys. Res., 97,* 14,249-14,257, 1992.

Trump, C. L., S. J. Neshyba, and W. V. Burt, Effects of mesoscale atmospheric convection cells on the waters of the East-China Sea, *Boundary Layer Meteorol., 24,* 15-34, 1982.

Ufermann, S., Untersuchungen zur Radar-Abbildung ozeanischer und atmosphärischer Phänomene an der Meeresoberfläche, diplom thesis, 99 pp., Univ. of Hamburg, Hamburg, Germany, Feb. 1998.

Ufermann, S., and R. Romeiser, A new interpretation of multifrequency/multipolarization radar signatures of the Gulf Stream front, *J. Geophys. Res.,* this issue.

Valenzuela, G. R., Theories for the interaction of electromagnetic and ocean waves—A review, *Boundary Layer Meteorol., 13,* 61-85, 1978.

Wright, J. W., A new model for sea clutter, *IEEE Trans. Antennas Propag., AP-16,* 217-223, 1968.

R. Romeiser, Institute of Oceanography, University of Hamburg, Troplowitzstraße 7, 22529 Hamburg, Germany. (romeiser@ifm.uni-hamburg.de)

S. Ufermann, Southampton Oceanography Centre, School of Ocean and Earth Science, European Way, Southampton, SO14 3ZH, United Kingom. (ufermann@soton.ac.uk)

(Received October 7, 1998; revised June 2, 1999;
accepted July 21, 1999.)